Geophys. J. Int. (2004) **159,** 591–606 doi: 10.1111/j.1365-246X.2004.02444.x

Geometry of extensional faults developed at slow-spreading centres from pre-stack depth migration of seismic reflection data in the Central Atlantic (Canary Basin)

T. J. Reston,[1] C. R. Ranero,[1] O. Ruoff,[1] M. Perez-Gussinye[1,*] and J. J. Dañobeitia[2]

[1]*IFM-GEOMAR, Leibniz-Institute for Marine Sciences, Wischhofstrasse* 1-3, D24148 *Kiel, Germany. E-mail: treston@geomar.de*
[2]*Institute of Earth Sciences, J. Almera, CSIC, Luis Sole i Sabaris s/n,* 08028 *Barcelona, Spain*

Accepted 2004 August 9. Received 2004 April 22; in original form 2003 January 20

SUMMARY

We present depth images, from portions of profiles that are close to flow-lines, of Cretaceous oceanic crust in the eastern Central Atlantic. Compared with post-stack time migrations, the images illustrate the improvement resulting from the application of pre-stack depth migration. The images document the scale and geometry of normal faulting in oceanic crust formed over 25 Myr at a half-spreading rate of less than 10 mm yr^{-1}, and the variation in extensional style with position within the spreading segment. Away from major fault zones (FZs), most faults are subplanar, dip more than 35°, are associated with moderate basement relief (0.2–1 km relief) and may penetrate to deep crustal levels. These faults could be related to the lifting of the lithosphere out of the median valley to the flanking mountains. Also observed away from FZs are gently dipping to subhorizontal reflections in the upper crust, which resemble detachment faults. In contrast, the inside corner crust is more rugged, with basement highs rising up to 2 km above the intervening basins. This larger-scale topography is associated with a different style of faulting: the depth images reveal gently dipping (<35°) faults that are rooted in the deep crust and that project to the ridgeward flank of the dome-shaped large basement highs (1–2 km vertical relief). The faults seem to continue as the ridge-facing flank of these highs and some may extend over the crest of the high to breakaways beyond. In this case, the domal highs that form the exhumed footwall to the faults can be described as oceanic core complexes. These controlling faults are up to 20 km long and have a heave of ∼10 km, sufficient to have accommodated up to 50 per cent extension and to have exhumed deep crustal and perhaps even mantle rocks. We suggest that similar faults can explain the structure and lithologies found at megamullion structures (oceanic core complexes) at inside corners near the present-day spreading ridge.

Key words: mid-ocean ridges, normal faulting, oceanic crust, seafloor spreading, seismic structure.

1 INTRODUCTION

Slow-spreading centres are strongly segmented (Macdonald *et al.* 1991) by transform faults and non-transform ridge-axis discontinuities. Crustal thickness increases towards the centre of the segments, whereas lithospheric thickness increases towards the segment ends (e.g. Cannat *et al.* 1995). Whereas the middles of segments are approximately symmetric, the ends of segments commonly exhibit a strong asymmetry between the inside corner and the outside corner (Fig. 1).

This segmentation exerts a strong control on the relative contributions of magmatic addition and tectonic extension to overall spreading (e.g. Gente *et al.* 1995). At the centre of spreading segments, magmatism is dominant, whereas towards the segment ends, large-offset faults become increasingly important, particularly at inside corners (adjacent to the active transform). Earthquakes are consistent with normal faulting (Bergman & Solomon 1984), striking parallel to the ridge axis and dipping at *ca.* 45° at the edge of or beneath the median valley (e.g. Huang & Solomon 1988; Toomey *et al.* 1988), extending to deep crustal levels and even into the mantle (Toomey *et al.* 1988), lifting newly formed crust out of the axial valley (Shaw & Lin 1993) and accommodating between 10 and 20 per cent of plate separation (Solomon *et al.* 1988). Bathymetric data show that faults are dominantly ridge-parallel and inward-dipping (towards the ridge) and control the formation of the abyssal hill morphology of the ridge flanks (Carbotte & Macdonald 1990; Shaw & Lin 1993; Escartin *et al.* 1999). Normal faults increase in offset and length but decrease in number towards the ends of

*Now at: Department of Earth Sciences, University of Oxford, UK.

individual segments (Shaw & Lin 1993): the faults with the greatest throw are associated with oceanic core complexes at inside corners (Fig. 1) adjacent to transform faults (Tucholke & Lin 1994; Cann *et al.* 1997) and other ridge-axis discontinuities (Tucholke *et al.* 1997a, 1998), the trace of which we describe as short-offset fracture zones (SOFZ). Here the largest faults may be responsible for the exhumation of deep crustal and mantle rocks at slow-spreading ridges (Tucholke & Lin 1994).

Studies of ophiolites (e.g. Dilek *et al.* 1998) also contribute to the understanding of faulting at mid-ocean ridges, but are overprinted by deformation associated with ophiolite obduction, and may not represent typical oceanic crust. Ophiolites formed at slow-spreading centres are in particular often incomplete, which may, however, reflect the processes occurring at the spreading centre (Lagabrielle & Cannat 1990) rather than dismemberment during emplacement. Despite the problems, comparisons have been drawn between the Troodos ophiolite and faulting in the MARK area (Dilek *et al.* 1998), as well as reflection images from Blake Spur (Agar & Klitgord 1995). In particular, both steep normal faulting and detachment faults (e.g. Allerton & Vine 1987; Agar & Klitgord 1995) of various types have been recognized.

Despite the wide variety of data about normal faulting at mid-ocean ridges, controversy remains about, for instance, the geometry of faults at depth, the relationship between steep faults and detachment faults, and the mechanism of detachment faulting. Some recent models for faulting at slow-spreading centres are shown in Fig. 1. For instance, Cann *et al.* (1997) discuss two possible geometries of the faults forming the corrugated domal surfaces exposed near high inside corners: they suggest that they may be convex-up structures cutting deep into the crust (Tucholke & Lin 1994) or may flatten at shallow levels and represent serpentinite-lubricated landslides. Mitchell *et al.* (1998) point out that, even if the slip surface does continue to depth, it may do so at a shallow or a steep angle. Similarly, there is debate about whether steep normal faults detach onto detachment faults active at low angle (e.g. Agar & Klitgord 1995; Reston *et al.* 1996b) or whether the steeper faults and the underlying 'detachment faults' form a rolling-hinge system (Buck 1988; Reston *et al.* 1996b).

One reason that the detailed geometry of normal faulting at depth remains a source of debate is the failure of seismic reflection data collected at the spreading centre to image the major structures. As discussed by Detrick *et al.* (1990), scattering of energy at the rough seafloor near the spreading axis prevents the imaging of the deeper structure. As a result, most seismic reflection studies of oceanic crust that formed at slow spreading rates (e.g. McCarthy *et al.* 1988; White *et al.* 1990; Banda *et al.* 1992; Mutter & Karson 1992; McBride *et al.* 1994; Ranero *et al.* 1997) have been away from the spreading axis, in regions where seafloor topography has been smoothed by the deposition of thick sedimentary sequences. These studies have imaged reflections dipping dominantly towards the spreading centre and associated with offsets of top basement, and hence interpreted as normal faults. Those faults that have been mapped in three dimensions (McBride *et al.* 1994; Collier *et al.* 1998) are roughly parallel to the ridge axis (see also Escartin *et al.* 1999) and laterally continuous for tens of kilometres. However, most previous studies have been based on time sections or on depth conversions of time migrations and have therefore not revealed the true geometry of the faults, nor their detailed relationship to top-basement morphology. In this paper we present and discuss images of faults produced by applying pre-stack depth migration to portions of seismic profiles (Fig. 2) over crust formed in the Central Atlantic during the Early Cretaceous (magnetic anomalies M0–M16, see Fig. 3) at a half-spreading rate of 7–10 mm yr^{-1}. The structures imaged probably formed at the spreading centre, and, by analogy with patterns of faulting observed near the spreading centre, probably strike parallel to isochrons. As the profiles discussed are close to flow-lines, they provide a fossil record of seafloor-spreading processes and in particular of normal faulting occurring between 145 and 120 Ma (Kent & Gradstein 1985).

2 DATA AND METHODS

2.1 Data acquisition and setting

The seismic reflection data used for this study were selected from three transects (A, B and C, see Fig. 2) comprising over 2000 km

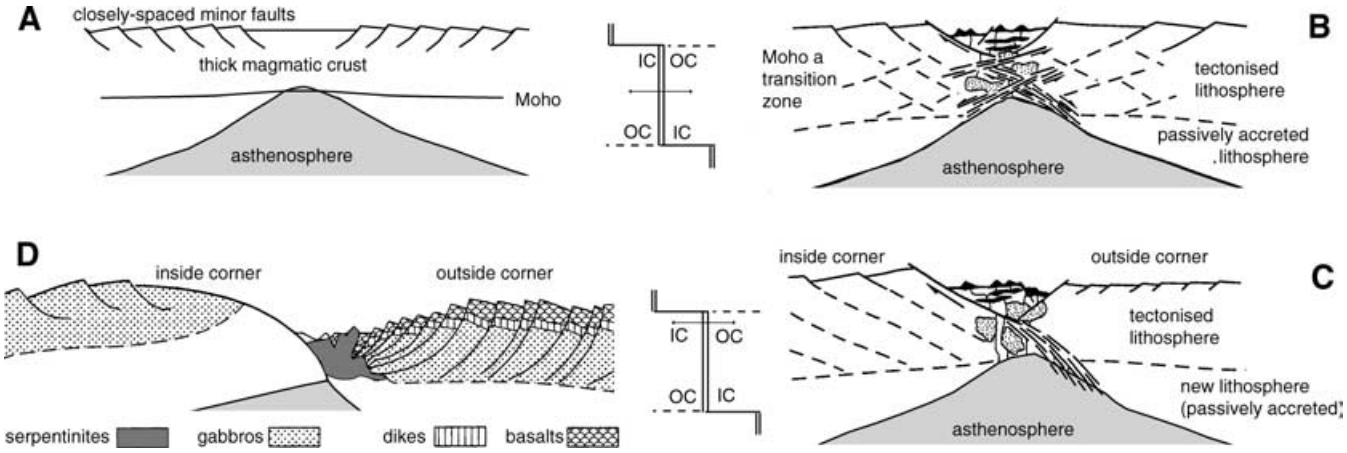

Figure 1. Schematic sections across the spreading centre, based on observations at or near the spreading axis. A and B denote symmetric spreading across the segment middle, for robust magmatic spreading (A—after Cannat 1996), and for relatively low melt production during spreading (B—modified from Lagabrielle *et al.* 1998), leading to unroofing of mantle rocks, perhaps accommodated by conjugate faults and shear zones. C and D denote asymmetric spreading across the segment end. C: steady-state model (Lagabrielle *et al.* 1998), in which low melt production results in continual mantle unroofing; D: cyclic model (Tucholke & Lin 1994), in which magmatic followed by amagmatic spreading phases lead to unroofing of a complete crustal section and of mantle rocks (minor faults cutting the main fault surface are successor faults caused by footwall flexure). Note that in all models the topography of the oceanic basement is controlled by normal faulting and that the exhumed slip surface is exposed as fault scarps.

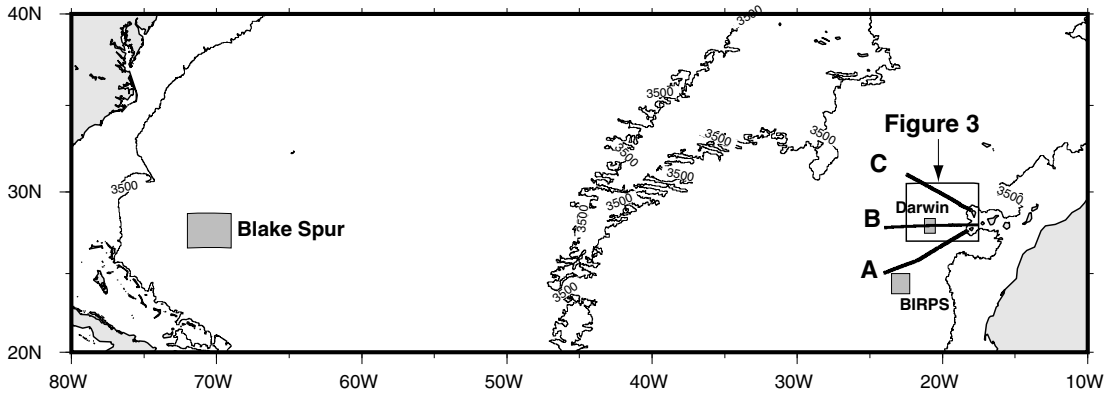

Figure 2. Map of the Central Atlantic showing the location of the study. Thick lines—Canary Basin profiles: in this study we concentrate on portions of Profiles B and C that are close to flow-lines. Shaded boxes—areas covered by BIRPS OCEAN survey (White *et al.* 1994), by Blake Spur profiles (Morris *et al.* 1993) and by Charles Darwin data (Collier *et al.* 1998). The area of Fig. 3 is marked by the open box.

of multichannel data collected by the commercial seismic vessel *Geco Tau* in 1988 (Banda *et al.* 1992; Ranero *et al.* 1997). The source consisted of a tuned array of 34 airguns (total capacity 105 litres) fired every 50 m. The signals were received by a 3000-m long, 120-channel analogue streamer, and recorded to 16-s TWT at a 4-ms sample interval. Banda *et al.* (1992) described the results of the standard processing of these data, which included a Wiener wavelet-shaping filter, velocity analysis and normal moveout (NMO) correction, common-midpoint (CMP) stack, and frequency filtering, whereas Ranero *et al.* (1997a) reported additional results of a constant-velocity (frequency–wavenumber) migration.

In this paper, we present the results of reprocessing, including pre-stack depth migration, of 240 km of these data (Fig. 3) taken from the portions of the transects B and C over crust formed between anomalies M0 and M16 (that is, between 120 and 145 Ma): both profiles are within 15° of flow-lines in the study region.

Most of the reprocessed data are located within individual segments between fracture zones, although the reprocessed portion of Profile B crosses a minor short-offset fracture zone (SOFZ—Hierro FZ, see Fig. 3). SOFZs can die out to zero offset (when they no longer act as segment boundaries) and reappear with a reverse sense of offset (Schouten & White 1980; Tucholke *et al.* 1997a). Consequently, in places it is not clear if Profile B runs along crust formed at a segment centre, or adjacent to a SOFZ. The location of Profile C relative to segment boundaries is, however, unequivocal as it runs along a large free-air gravity high on the inside corner (IC) side of a fracture zone characterized by 30 km of dextral offset (Ranero *et al.* 1997; Ranero & Reston 1999).

On 2-D profiles there is always uncertainty about the true orientation of the structures imaged. Of the features described here, for some (e.g. F4) we do have 3-D control because of local grids of data; for most of the others we have clear evidence from velocity pull-ups that the reflections come from within the basement beneath or almost beneath the profiles.

2.2 Pre-stack depth migration

Pre-stack depth migration (PSDM) offers the possibility of improved imaging in regions of complex structure and/or strong velocity contrasts. In such settings, standard processing suffers from CMP smearing, does not allow for ray-path bending, and suffers from velocity distortions. The strong velocity contrast between the sedimentary layers (velocities generally between 2 and 3 km s^{-1}) and igneous basement (velocities >4.5 km s^{-1}) coupled with the rough topography of the top basement mean that the method can greatly improve resolution in the upper oceanic crust and remove velocity pull-up effects. The method can also, in regions of strong reflectivity, deliver high-resolution velocity information (Reston *et al.* 1996a). Processed data portions (including spherical divergence correction, time-variant frequency filtering and resampling to 8 ms) were pre-stack depth migrated using two different schemes. First, a relatively quick Kirchhoff algorithm was used iteratively to build up a velocity model using depth-focusing error analysis (Denelle *et al.* 1986). After the construction of final velocity models, a more computer-intensive but somewhat higher-resolution finite-difference scheme was used to produce the final sections.

The velocity model is of high resolution and laterally variable within the layered sedimentary sequence, allowing the accurate imaging of top igneous basement. Within the basement, however, it is constrained by depth-focusing error analysis only where strong reflections are present (Reston *et al.* 1996a,b). These gave velocities consistent with the known velocity structure of oceanic crust of this age (White *et al.* 1992), whereas side-coming energy generally gave anomalously low interval velocities. Such artefacts could also generally be distinguished from genuine intracrustal reflections on the basis of the velocity pull-ups on time sections evident for the latter (Ranero & Reston 1999). Furthermore, we have used the dip-moveout (DMO) method (Kent *et al.* 1996; Reston *et al.* 1999) to distinguish between side-swipe energy and genuine intracrustal reflections (Ranero & Reston 1999).

The final velocity models generally show a 'layer 2' (velocity increasing from *ca.* 4.5 km s^{-1} at top basement to $\sim$ 6.5 km s^{-1} 2 km beneath top basement— Ranero & Reston 1999) underlain by 'layer 3' (velocity increasing from just over 6.5 km s^{-1} to just over 7 km s^{-1} by $\sim$7 km beneath top basement). No velocity step was introduced at the layer 2–3 boundary as this is generally thought to be a change in velocity gradient (Spudich & Orcutt 1980) rather than a step, nor at the Moho because this was generally not marked by a strong reflection and so could not be picked with confidence. The intermittent reflectivity of the Moho may reflect its variable nature in slow-spread oceanic lithosphere: a boundary between crust and mantle in places and a transition (probably less reflective) between serpentinized and unserpentinized mantle in others. In the absence of coincident wide-angle data, however, we cannot constrain the nature of the Moho further. By not introducing a velocity step at approximate Moho depths, we have avoided distorting images of

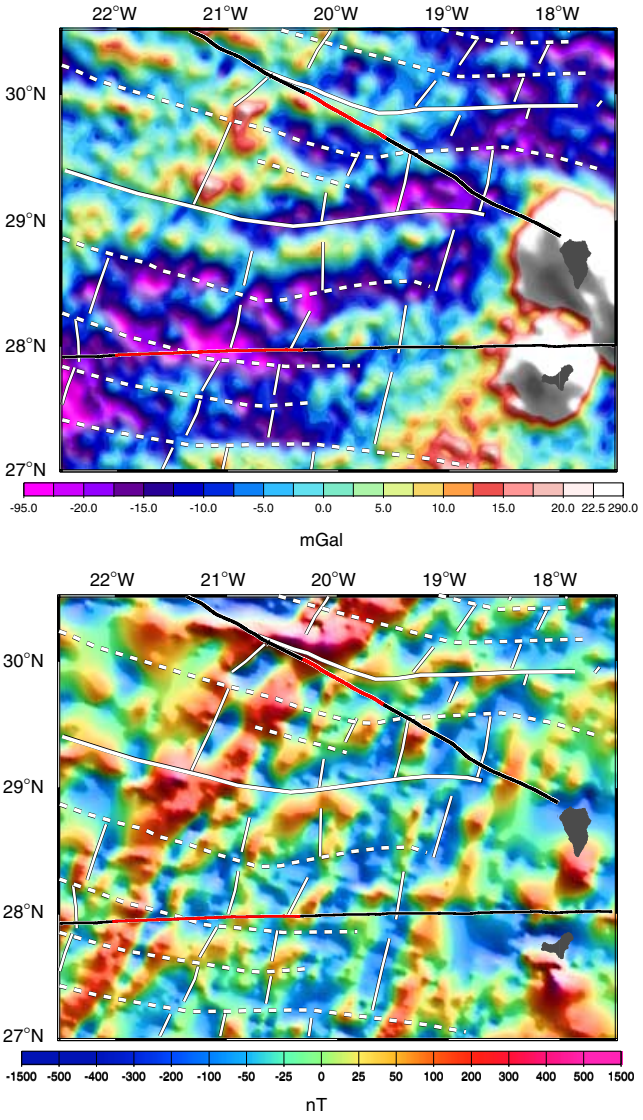

Figure 3. Potential field maps showing locations of profiles (black), and portions pre-stack depth migrated (thick black lines; red lines in the colour online version). (a) Free-air gravity (Smith & Sandwell 1995), showing selected magnetic anomalies (Roest *et al.* 1992) and fracture zones (Ranero *et al.* 1997): moderate-offset FZs as solid white lines, and short-offset (less than 20 km) FZs as dashed lines. Note that short-offset FZs need not be continuous structures and need not follow flow-lines. The seismic profiles studied were shot over crust of approximately the same age (M3–M16) and spreading rate (less than 10 mm yr^{-1} half-rate). (b) Magnetic map (not reduced to the pole—after Verhoef *et al.* 1996) of the same region: the magnetic picks (Roest *et al.* 1992) were actually based on reduced-to-the-pole data and provide constraints on the FZ offsets and spreading rates within the study area. Note that, whereas the studied portion of Profile B crosses a minor SOFZ, that of Profile C runs along a gravity high at the inside corner of a larger-offset FZ.

any crust that might have been below this step, but at the price of a minor distortion of any reflections in the mantle. As little reflectivity is observed in the deep section, this is not a significant problem.

The results of applying PSDM to the selected portions of the data are summarized in Fig. 4. The main improvement to the image, as illustrated in several comparisons below, is in the continuity of key reflections (particularly in the upper basement) and in the removal of pull-up effects apparent in the time sections. (These pull-up effects are useful, however, as evidence that the reflections come from the subsurface virtually beneath the profile rather than from the side.) Most important, by removing velocity distortions, the true geometries of the structures are revealed for the first time, clarifying the relationship between the faults and top basement.

Our results can be considered in two parts: those from Profile B located away from large-offset fracture zones (the trace of transform faults); and those from Profile C, which runs along the IC of a large fracture zone (∼30 km offset). The results from the two areas are quite different and may reflect differences in crustal structure related to the position of the profiles within Early Cretaceous spreading segments. As no automatic gain control (AGC) has been applied either before or after PSDM, the resulting images retain some information on relative amplitudes. In our interpretations we concentrate on the main features that we have been able to follow during the processing sequence, as we can be sure that these are not artefacts. As the focus of the paper is on normal faulting, we concentrate on those features that can be interpreted as normal faults (i.e. are associated with a suitable offset of top basement): this means that a wealth of other reflectivity (e.g. due to magmatic processes, hydrothermal alteration, or sedimentary processes) are not discussed in detail.

3 IMAGES OF CRUST AWAY FROM LARGE-OFFSET FRACTURE ZONES

We have pre-stack depth migrated 160 km of Profile B between magnetic anomalies M0 and M16 (Fig. 4). The eastern portion of the reprocessed line occurs 10–15 km north of the Hierro FZ, where this is marked by a ∼5 km dextral offset of the magnetic anomalies (Ranero *et al.* 1997; Collier *et al.* 1997, 1998). Here the profile runs over crust marked by a broad low in the free-air gravity and which formed either near the centre of a segment or at an outside corner to a second-order ridge-axis discontinuity, depending on distance from the FZ. Where the profile crosses obliquely at shotpoint (SP) 2500–2700 (Figs 3–5), the projected continuation of the Hierro FZ, there is no resolvable offset of the magnetic anomalies: here it is possible that the Hierro FZ has either disappeared or has close to zero offset. In contrast, south of the projected trace of the Hierro FZ, the satellite gravity is marked by a series of gentle highs, the flanks of which are crossed by the western portion of the reprocessed Profile B. We might thus expect a change in the type of crust and its seismic image at this FZ.

3.1 Steep normal faulting

The basement topography on Profile B (Fig. 4) is dominated by a series of step-like down-to-the-west offsets of up to 1 km vertical displacement. Between these steps, the basement dips gently down to the east at an angle of ∼5°, probably indicating the amount of back-rotation of the blocks. The basement highs are too large and too asymmetric to be volcanic constructions: we interpret the topography as generated by block-faulting at the spreading centre. The largest steps in top basement occur on average about 10 km apart (Fig. 4) and resemble normal block-faulted Mid-Atlantic Ridge bathymetry away from megamullions.

The region where the profile crosses the projected path of the Hierro FZ (Fig. 5) is characterized by two basement offsets of about 500 m vertically (SPs 2530 and 2680), each apparently down-to-the-west. From both west-facing scarps, west-dipping reflections (F1 and F2) can be traced down to the west, although F1 is not well imaged in the upper crust. F1 can be described as listric as

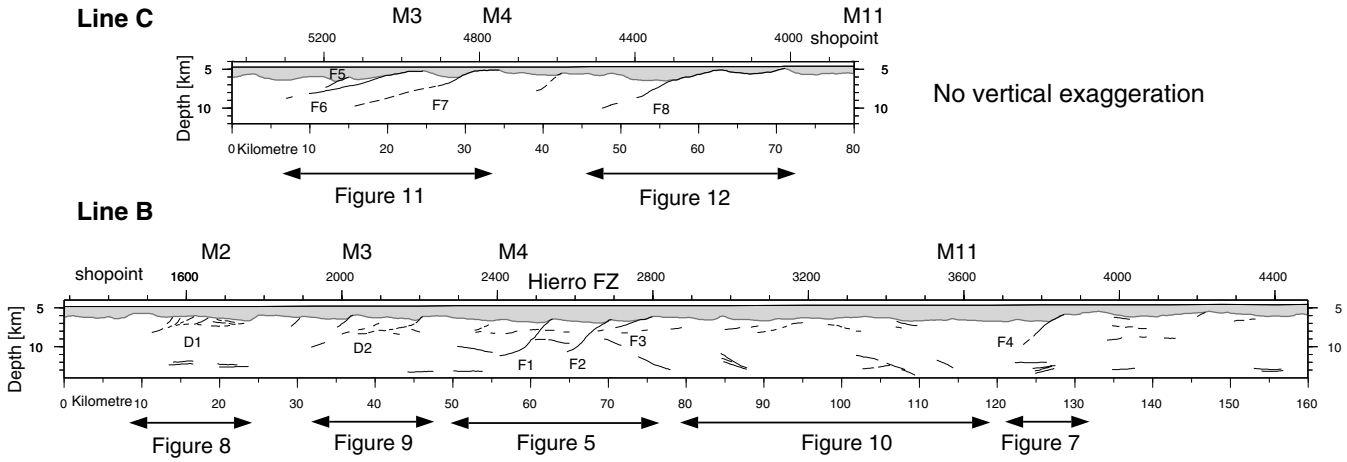

Figure 4. Line-drawings of the principal features discussed in the paper from the data depth migrated before stack (see Fig. 3 for locations of the profiles). The line-drawings are aligned at anomaly M4, and show the principal features observed on the data. Note the large offsets, crustal scale and 10–20 km spacing of the major faults imaged along Profile C: these imply considerable tectonic extension at the ridge axis. In contrast, faulting along Profile B (away from major FZs) is characterized by smaller heaves, implying less extension.

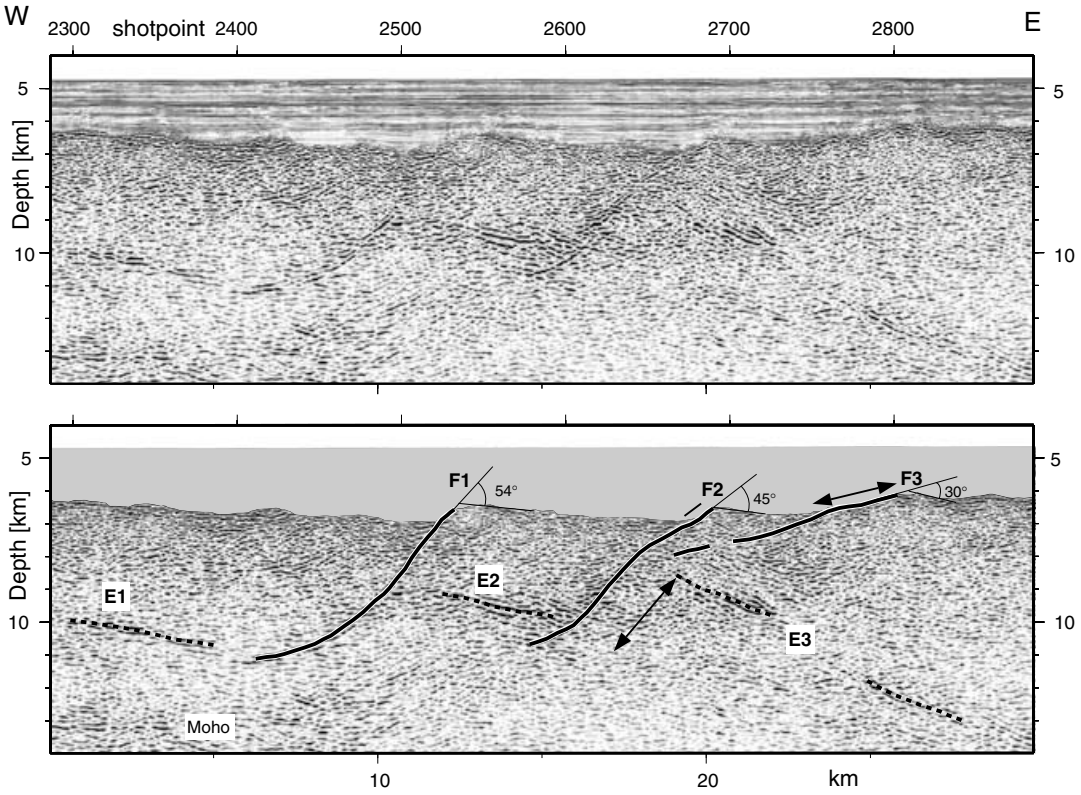

Figure 5. Portion of Profile B in the vicinity of the Hierro Fracture Zone (Ranero *et al.* 1997) depth migrated before stack. Two west-dipping structures (F1 and F2) can be identified in the vicinity of the inferred fracture zone and are interpreted as faults; a less-well imaged third dipping reflection just to the east (F3) is also probably a fault. F1 and F2 appear to cut and truncate east-dipping reflections (E1, E2 and E3). Restoring the slip on F2–F3 (lines and arrows show displacement along various portions of the fault system) brings E3 into alignment with E2. We tentatively identify the E reflections as the crust–mantle boundary in a region of thinned crust associated with the fracture zone. Note that, where present, the Moho reflection lies deeper: the lower crust may be dominantly serpentinized peridotites.

it steepens upwards from ∼10° at about 11 km depth (4–4.5 km beneath top basement) to ∼40°–50° at about 8 km depth (∼1 km beneath top basement). F2 appears more S-shaped, being steepest 3–4 km beneath top basement and flattening slightly both downwards and upwards to intersect top basement at about 30°. Because of their association with the offset of top basement, we interpret the apparently west-dipping intracrustal reflections as faults, in common with other authors (e.g. McCarthy *et al.* 1988; Banda *et al.* 1992; McBride *et al.* 1994; Ranero *et al.* 1997). We are aware that structures in the vicinity of a second-order ridge-axis discontinuity may not strike normal to the spreading direction, implying that our profile may not image the true geometry of structures here. More

specifically, it is possible that the structures are somewhat steeper than indicated in the depth section, but, as both F1 and F2 already appear as steep structures on the section, even if they are oblique to the profile their true geometry can only be slightly steeper. A third, more gently dipping and less-well imaged structure (F3) cuts down to the west from a basement high at SP 2800: this too we interpret as a fault that stops at the steeper F2. Various other possible faults (e.g. between F1 and F2 there is an apparently more gently dipping structure) may be present. One possible interpretation of this is that the faults F2 and F3 form a rolling-hinge system (Buck 1988). In this F3 was first active, but flexurally rotated to such a low angle that the upper portion of F3 became inactive, so that a new steeper fault (F2) propagated up from the root zone.

The generally west-dipping faults associated with the Hierro FZ region appear to truncate and offset east-dipping features within the basement (Fig. 5). These structures, labelled E1, E2 and E3, cannot be traced to the top of the basement, and so are unlikely to represent faults. The easternmost of the three (E3) extends to depths expected for the Moho, although no clear Moho reflections are imaged beneath the fracture zone. We speculate that these east-dipping reflections may represent the crust–mantle boundary, that is the boundary between igneous basement and perhaps serpentinized peridotites. (It is unlikely that these reflections mark the top of unserpentinized mantle as there is a gravity low not a gravity high associated with the Hierro FZ.) This would imply that structures F1 and F2 cut down through the crust–mantle boundary (CMB) in this region of thin crust. At first glance, it appears that the heaves of these faults indicate insufficient movement to have thinned the crust significantly, implying that the thinning observed may instead here be related to limited melt supply near the Hierro ridge-axis discontinuity. As discussed further below, however, if F2 and F3 form a rolling-hinge system, movement along these faults may together have led to sufficient crustal thinning to have brought mantle rocks near to the surface.

Minor faults appear to have disturbed the sedimentary cover, particularly in the vicinity of the fracture zone. The throws on these faults are, however, extremely small compared with those that offset top basement. Little sediment appears to have been deposited during the development of the basement topography, as the sediments do not form wedges fanning towards the faults. We thus conclude that the faulting evident in the sediments represents at most only a very minor reactivation of the basement faults and might be explained by differential compaction. The basement faults themselves formed when no resolvable sediment had been deposited, i.e. close to the spreading centre. As the sediment clearly post-dates the main faulting and the formation of the underlying basement, in this and other sections the layered sedimentary succession has been blanked out to emphasize the relationship of faulting to basement topography.

Further east still, the end of a region of smooth basement (see below) is marked by a major offset of top basement at SP 3850 (Figs 6 and 7)—here a west-facing basement scarp with a vertical offset of slightly more than 1 km is observed. On the time section (Fig. 6, top), it appears that the west-facing scarp is considerably steeper than the fault within the basement, although the scarp itself is not imaged. However, on the depth section (Fig. 6, middle and bottom), both the scarp and the true geometry of the faults are revealed. Within the basement, the fault appears as a west-dipping planar to slightly convex-up reflection (F4—but see Section 5.2 below) that can be confidently traced down to a depth of at least 2.5 km beneath top basement (depth ∼9 km), where it has a dip of ∼40°. If all faults formed at or near the spreading axis, F4 formed

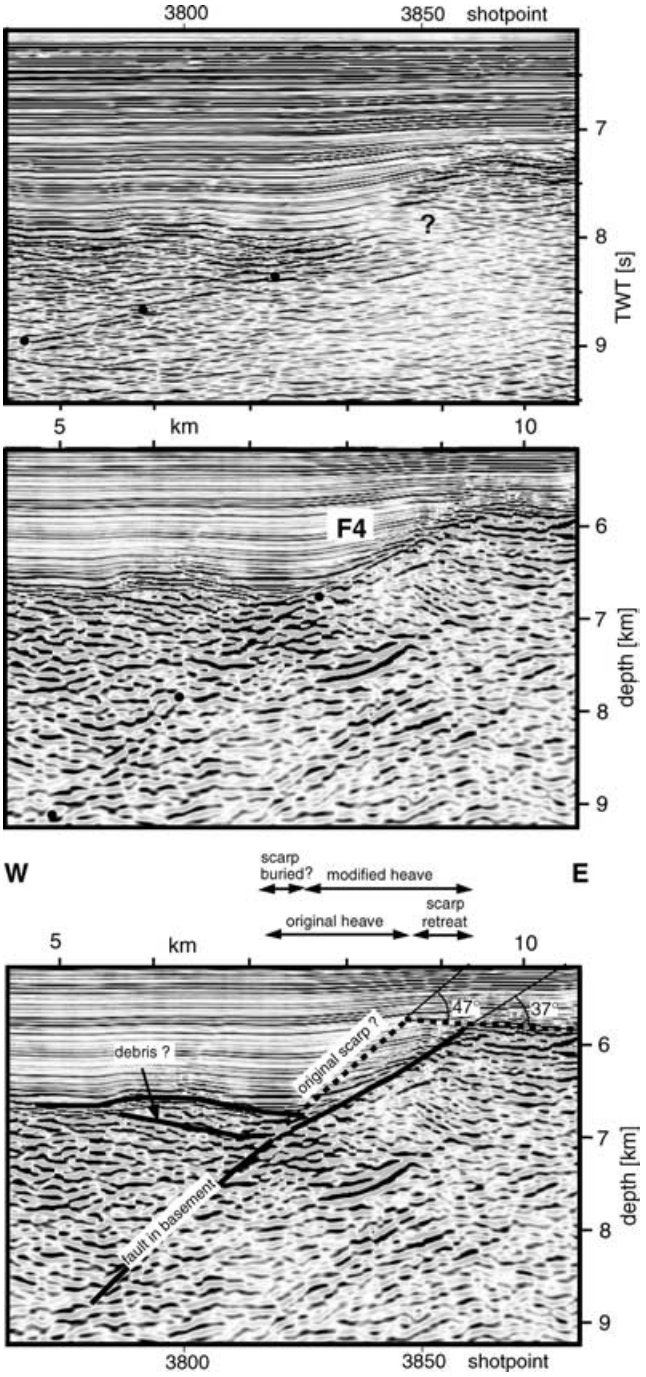

Figure 6. Portion of Profile B (see Fig. 7 for location), showing details of fault F4 and its relationship to top basement. Top: time migration (Ranero *et al.* 1997). Note that the fault scarp is not well imaged but appears far steeper than the fault F4 within basement, marked by dots. Middle and bottom: pre-stack depth migration, showing how the scarp (onlapped by the sedimentary fill) is actually slightly less steep than the portion of the fault in the basement; the fault scarp appears slightly concave, consistent with its modification by mass-wasting. In estimating heave from faults such as this it is necessary to first reconstruct the fault geometry by extrapolating the fault up from the basement. In this example we show two estimates, assuming in one that landsliding and mass-wasting have not occurred and in the other that they have, producing a wedge of rubble. Such details evident on the pre-stack depth migration are not apparent on the post-stack time migration.

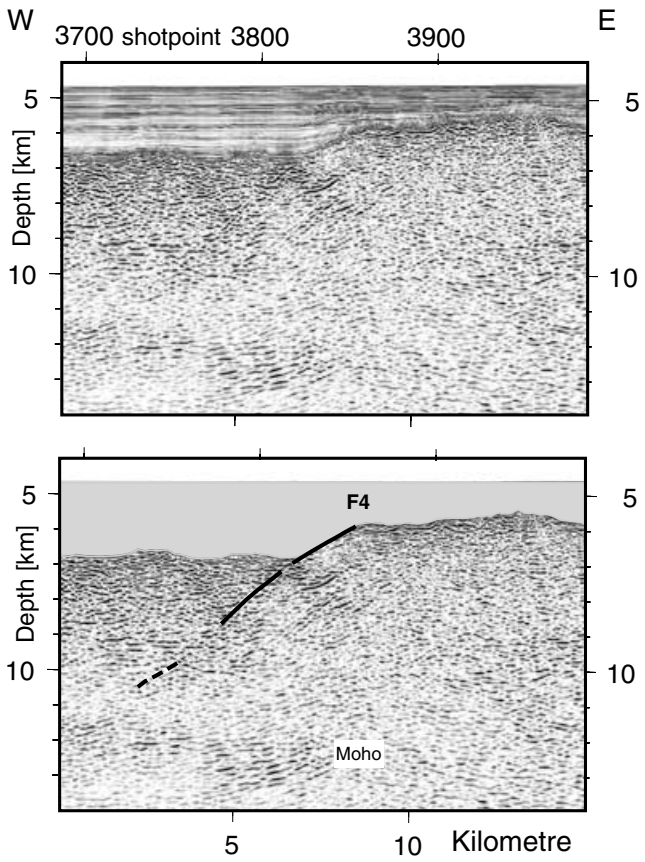

Figure 7. Portion of Profile B (pre-stack depth migrated) showing the continuation of F4 to depth and possible Moho reflections. See Fig. 4 for location.

~5 Myr before F3. Upwards, F4 can be traced to the basement offset: approaching top basement F4 appears to flatten gradually to about 35° and appears to be continuous with the convex-up west-facing flank of the basement high. The west-facing scarp (now onlapped by post-spreading sediment) dips more gently (~30°), but may not be the original fault scarp as discussed further below, but rather the product of mass-wasting. A possible wedge of debris is imaged at the foot of the scarp on the depth section, but not on the time section.

Deeper in the section (Fig. 7), the fault may be marked by the truncation of subhorizontal reflections in the hangingwall at about 9–10 km depth, and by weak west-dipping reflections just below 10 km and 11–12 km depth (fault plane reflections?). The fault can thus be traced to 9 km, and possibly to a depth of 12 km (5 km beneath top basement, i.e. deep within the crust, a Moho reflection can be tentatively interpreted on this section), where it has a dip of about 30°. The F4 structure has been mapped out using a series of short flow-line profiles (Collier *et al.* 1998), which confirm that it is a genuine intracrustal reflection, dipping towards the spreading centre. The apparent cross-cutting relationship between the west-dipping fault plane reflection and a horizontal event at ~7.5 km is thus curious, and might imply that the subhorizontal reflection comes from out of the plane of section. Alternatively, the relationship might indicate that the subhorizontal reflection developed in the basement after movement on F4 ceased. Similar subhorizontal reflections have been interpreted as hydrothermal fronts (Minshull 1993) and fractures associated with fluid flow (Hallenborg *et al.* 2003)—hints of such subhorizontal features are present in several places on our profiles, but are not discussed further here.

3.2 Detachment faulting

In addition to the moderately steep faults described above, a number of low-angle structures are imaged in the upper crust after application of PSDM. For instance, very gently west-dipping reflections (D1) can be traced to the west from a west-facing flank of a basement high at SP 1765 (Fig. 8). These become subhorizontal or even slightly east-dipping ~1 km beneath top basement (SPs 1600–1700) before merging with a steeper reflection at SP 1565 and cutting further down to the west towards SP 1500. These reflections can be traced in total over about 10 km and may mark the lower limit of faults that appear to cut down from small offsets of top basement at SPs 1660 and 1690. The westernmost of these two faults above D1 is marked by a weak west-dipping reflection; the eastern one, by the termination of reflections in both the hangingwall and the footwall. On the time migration (Ranero *et al.* 1997), D1 is barely imaged, appearing as a series of weak reflection segments smeared by CMP-stacking and affected by velocity pull-up beneath a broad arching of the top basement. (Such pull-up does help indicate that the reflection comes from within the basement rather than from the side.) The improvement offered by the depth image is particularly pronounced near SP 1700.

The relationship between the D1 reflection and the offset of top basement at the east end of the section is not clear on the time migration, but in the depth section D1 can be traced down as a continuous feature from the same basement scarp, which is now imaged as a west-dipping reflection. This illustrates the improvement achieved by PSDM in the image of top basement and beneath the strong velocity contrast at top basement. Partly on the basis of the association of D1 with a clear basement offset, we interpret D1 as a detachment fault onto which more steeply dipping faults appear to detach. D1 resembles detachment faults observed at rifted margins and in highly extended continental regions (e.g. Lister & Davis 1989; Buck 1988; Reston *et al.* 1996a). Structures (also interpreted as detachment faults) similar to D1 are imaged (Reston *et al.* 1996b) on flow-line profiles shot north of a minor offset in the magnetic anomalies in the Cape Verde Abyssal Plain to the south (Henstock *et al.* 1996). Two possible interpretations are possible (Reston *et al.* 1996b): either the detachment was active at low angle (and the small, overlying faults really do detach onto it), or it forms a rolling-hinge system (Buck 1988) in which only the steepest, youngest (in this case, most westerly) portion is active at any one time (Fig. 6), and the 'detachment' of the overlying faults onto an underlying master structure is misleading.

On the depth section, the small basins developed above the D1 detachment fault appear to be characterized by small zones of bright reflectivity, overlain by unequivocal sedimentary units. These reflective zones, not resolved on the time migrations, might consist of lava flows separating rubble and debris generated by disaggregation and perhaps some mass-wasting (e.g. Tucholke *et al.* 1997b) of the volcanic crust and locally infilling rift-generated topography. The dimensions of these reflections (1–2 km) are similar to that of lava flows described from the modern Mid-Atlantic Ridge (MAR) (Smith & Cann 1990). The detailed structure of the upper plate fault blocks resting on D1 is, however, poorly imaged, making estimates of the amount of extension associated with this system problematic.

Other low-angle structures are imaged within the upper crust on this profile, and may also be detachment faults, albeit not so clearly imaged. For instance, slightly further east a weak, west-dipping reflection (D2) appears to cut down to the west from an offset in top basement at SP 2200 (Fig. 9). It flattens to less than 10° about 1.5 km beneath top basement, before merging with a steeper

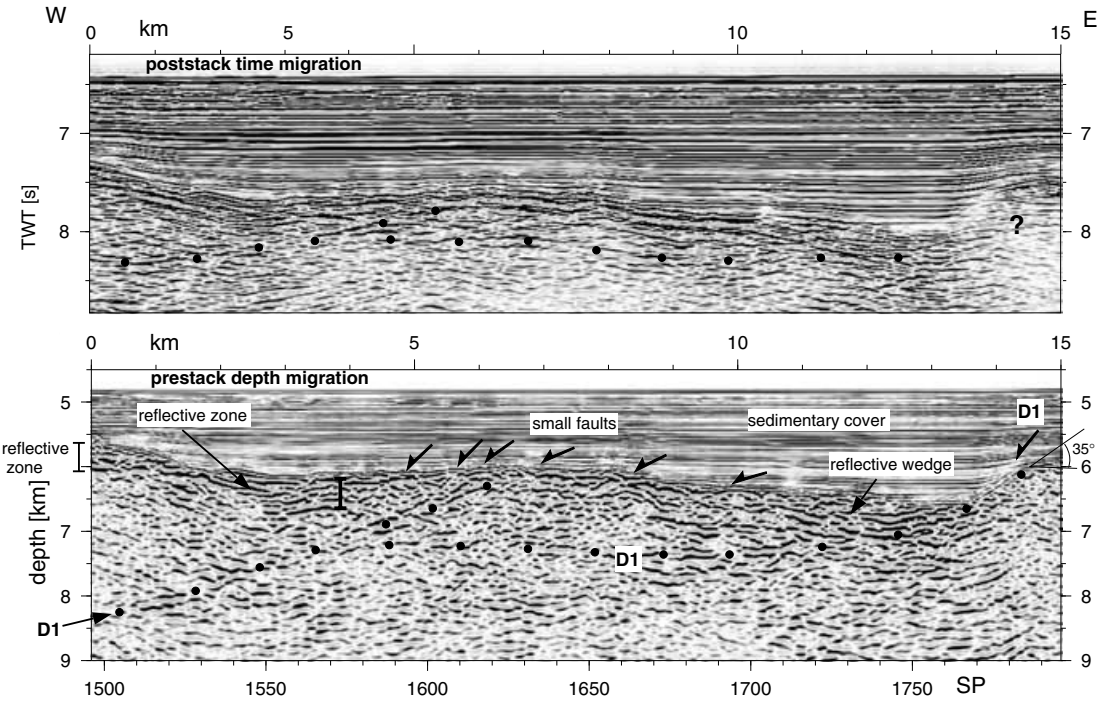

Figure 8. Detail of Profile B. Top: post-stack time migration (Ranero *et al.* 1997), showing poor imaging in the upper 500 ms of basement. Location of D1 (as interpreted from the depth migration) is marked by dots. Middle: image from pre-stack depth migration, showing a greatly improved image in the top 1 km of basement. A series of gently dipping upper crustal reflections (D1) cut down from a basement offset at SP 1765, flatten ∼ 1–1.5 km beneath top basement, and merge at 1 km beneath top basement with a steeper structure (dipping ∼ 25°) at SP 1560. The subhorizontal reflection is interpreted (bottom) as a detachment fault, probably formed by a rolling hinge as discussed in the text. The basement above D1 appears to be cut by faults too small to be imaged completely. High reflectivity in the uppermost crust of the depth migration (not apparent on the time migration) may represent a zone of disaggregated volcanics and sediment, intercalated with flows (e.g. Smith & Cann 1990). Between SPs 1650 and 1750 this thickens to the east, defining a half-graben in the hangingwall of the main D1 structure. D1 intersects top basement at an angle of ∼35°, which may represent its original dip at the seafloor.

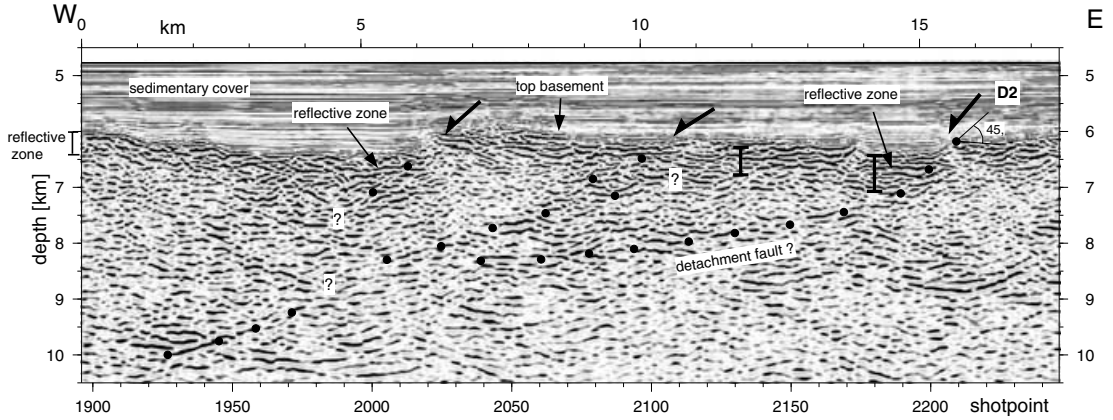

Figure 9. Detail of Profile B (pre-stack depth migrated), showing a currently listric upper crustal structure (D2) cutting down from a basement offset at SP 2200. The dip of the features shallows to the west to ∼ 15°; at SP 2000 and ∼ 2 km beneath top basement it merges with a steeper west-dipping structure which cuts to 5 km beneath top basement (SP 1920). We interpret the low-angle structure as a form of detachment fault (D2) and infer that at its intersection with the surface it originated with a dip of perhaps 45°. Its current listric geometry is probably a result of the unloading of the footwall due to the extension of the hangingwall.

structure at ∼2 km beneath top basement at SP 2000. The continuation of these structures further west is not fully clear, although a deeper west-dipping reflection is imaged between 9 and 10 km depth (2.5–3 km beneath top basement). Here too we suggest that the gently west-dipping D2 reflection comes from a detachment fault onto which relatively minor west-dipping normal faults appear to sole: although these are not clearly imaged, they can be inferred from small offsets of top basement. The top basement is unusually reflective, perhaps also indicating a series of lava flows intercalated with rubble within the half-graben. Other weak, discontinuous low-angle reflections are observed north of the trace of the Hierro FZ (Fig. 10). One of these is associated with a minor offset of top basement and may also be a low-angle 'detachment fault', albeit poorly imaged. The nature of other upper crustal reflections within a generally reflective top 2 km of the basement on this portion of the profile is, however, less clear.

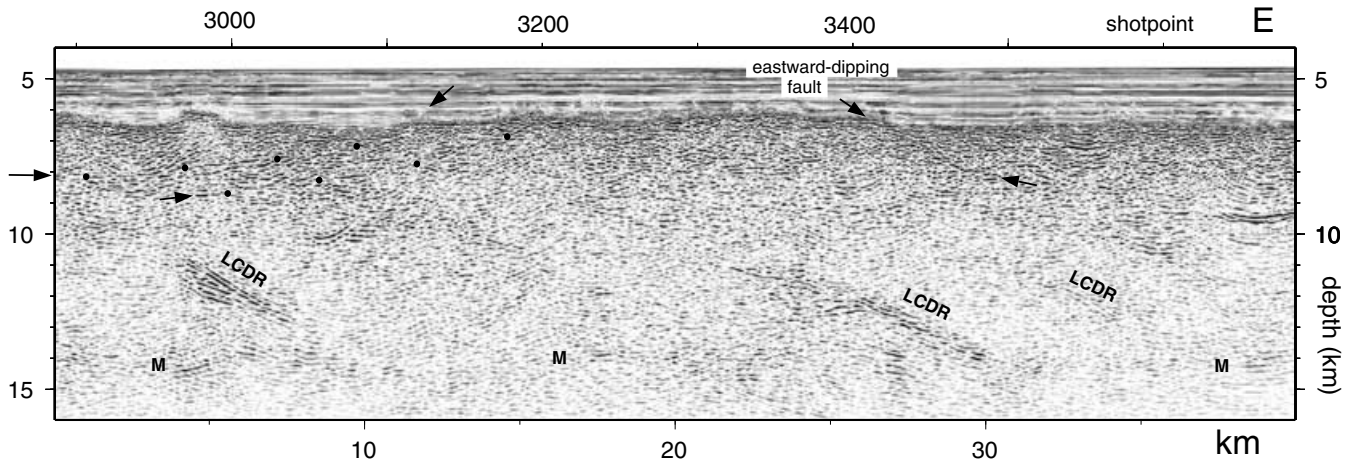

Figure 10. Portion of Profile B (pre-stack depth migrated), to the east of the Hierro Fracture Zone. Here the crust is unusually thick and topped by a broad expanse of relatively smooth basement. The upper 2 km of the crust is, however, generally moderately reflective. Two sets of gently west-dipping reflections are highlighted: one of these can be traced up to an offset of top basement and so might represent a low-angle normal fault. The lower crust is characterized by packets of east-dipping reflections, which we consider to represent a tectonomagmatic fabric within the deep crust, but not to be a classical fault. The Moho (M) is unusually distinct on this portion of the data. LCDR: lower crustal dipping reflections.

3.3 Smooth basement

In general, the crust to the north of the Hierro FZ (between F3 and F4, and also to the east of F4) is unusually smooth compared with that further west (south of the Hierro FZ—Figs 4 and 10). We suggest that the smooth crust between F3 and F4 probably formed by relatively robust magmatic construction and less faulting, during a spreading phase which lasted (assuming that both F4 and F3 formed at the spreading centre) ∼5 Myr. It is unclear, however, whether the contrast between the smooth crust and the more faulted basement further west is due to a westward decrease in the spreading rate, in degree of melting [the smooth igneous crust north of the Hierro FZ is 8 km thick in places (Collier *et al.* 1998), i.e. somewhat thicker than usual] or to small-scale segmentation of the spreading centre. The last could reflect a transition across the Hierro FZ from crust formed at an inside corner (south) to that formed at an outside corner (north). (It should be borne in mind that the Hierro FZ is a SOFZ that need not be associated with well-defined and temporally stable inside and outside corners.) Beneath the relatively smooth basement top, a series of weak discontinuous reflections, dipping west at about 15°, are imaged. Several of these are associated with minor down-to-the-west offsets of top basement and so these may be partial images of apparently low-angle faults.

Deeper in the section in Fig. 10, east-dipping lower crustal dipping reflections (LCDRs) are imaged. Unlike the E reflections described earlier, these are not discrete reflections but rather occur as packets up to 1 km thick. They cannot be traced upwards to offset of top basement. As a result, we do not interpret them as faults, as has been suggested by Collier *et al.* (1998). Furthermore, the LCDRs are not associated with thin crust as in the vicinity of Hierro itself, but rather with unusually thick crust (Collier *et al.* 1998), and so are unlikely to represent offset portions of the crust–mantle boundary as we propose for the E reflections. Unlike the E reflections they are not truncated upwards against clear west-dipping structures. Instead, we suggest that they represent some form of ductile or tectono-magmatic fabric within the deep crust but are beyond the scope of this paper. Similar, albeit ridgeward-dipping, LCDRs have been observed elsewhere in crust dominated by magmatic accretion (Reston *et al.* 1999; McCarthy *et al.* 1988).

Thus along Profile B we image moderately dipping normal faults (∼45°) and possible shallow, low-angle detachments within the basement. The topography of the top basement varies between clearly block-faulted regions, with steep west-facing scarps up to a kilometre high, and other portions of the profile where top basement appears little faulted.

4 IMAGES OF A FOSSIL INSIDE CORNER

We have reprocessed 80 km of Profile C between anomalies M2 and M11 (Figs 3 and 4). In this region, the profile is oriented at about 15° to a flow-line (Ranero *et al.* 1997), and does not cross any fracture zones, implying that the profile runs almost normal to structures formed within a single spreading segment. It does, however, run down the IC side of a relatively large-offset fracture zone [30 km of dextral offset in the magnetic anomalies (Ranero *et al.* 1997)], and along the axis of a large, fracture-zone-parallel linear free-air gravity high (Fig. 3), typical of crust produced at inside corners. We thus infer that the studied portion of this profile runs along crust formed at a Cretaceous IC (Ranero & Reston 1999). As such, the profile provides constraints on the internal structure and evolution of inside corners. We show here two adjoining portions of the profile as both time and depth sections.

Considerable coherent energy is apparent on the depth sections. However, some overmigrated features can be shown by depth-focusing error analysis to have anomalously low velocity and hence are probably reflections from out of the plane of section. These include the strong events observed beneath a basement high at SPs 4820–4740 at an apparent depth of about 8 km (Fig. 11). Because of the likely presence of such artefacts in the deep section, we have concentrated our interpretation on reflections that can directly be related to the basement topography imaged on the profile and which behave as real in-plane reflections during processing (see section on data processing).

The PSDM portion of Profile C (Figs 4, 11 and 12) is characterized by long-wavelength and large-amplitude basement topography, with up to 2 km vertical offset. Basement highs at SPs 4950, 4750, 4180 and 4010 are the most prominent, and are separated by deep

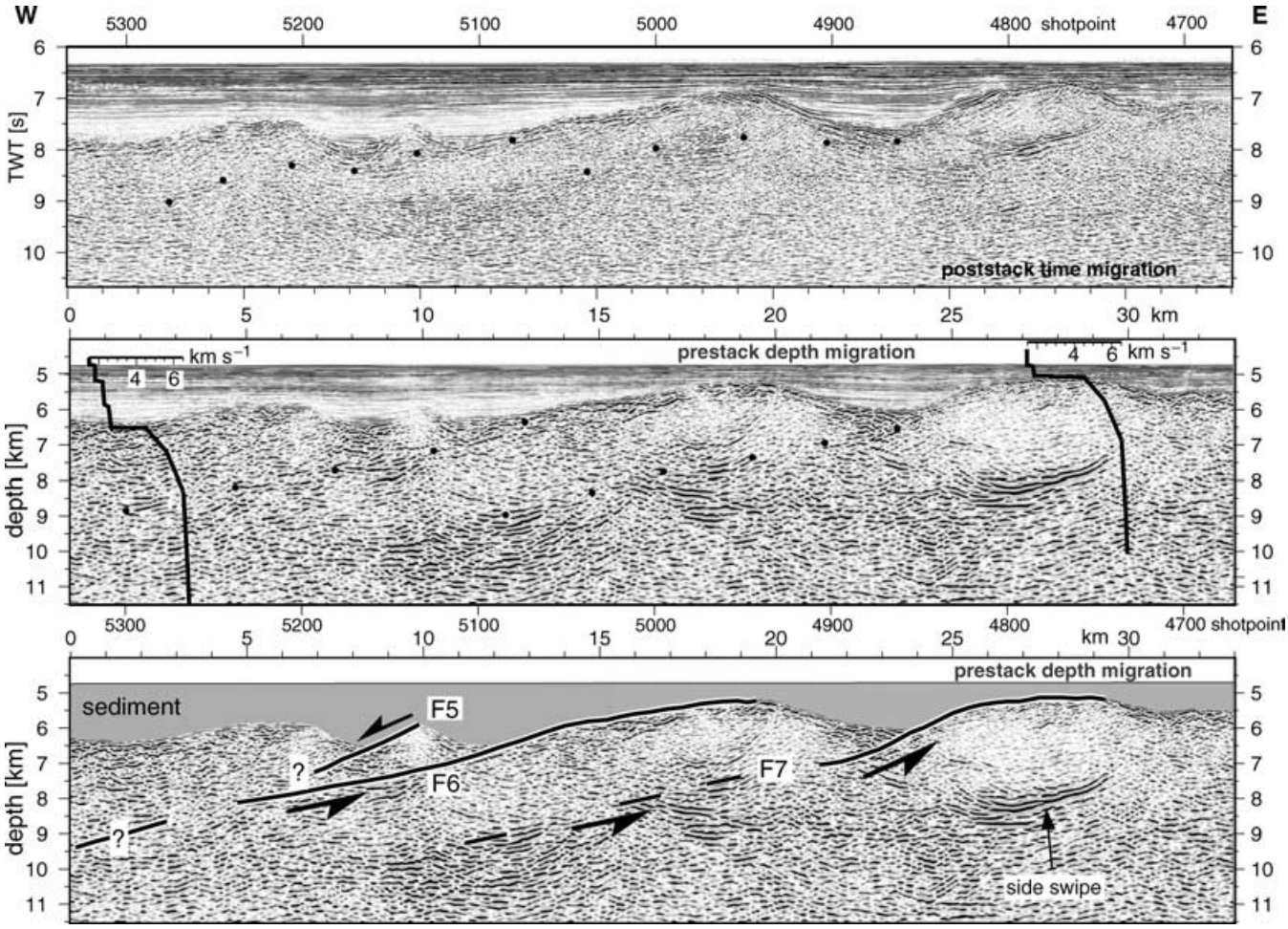

Figure 11. Portion of Profile C. Top: post-stack time migration. Middle: pre-stack depth migration showing the velocity model used in basement. Note that, whereas the sedimentary velocity model is detailed, that in the basement is simple and tracks top basement. Bottom: interpretation. A series of reflection segments defining west-dipping features (F6 and F7) can be traced to depth from the west flank of basement highs on the depth migration (middle); on the time migration (top) these features are strongly affected by velocity pull-up and can only be interpreted (dots) with reference to the depth migration. The F6 and F7 reflections are interpreted (bottom) as coming from normal faults, formed at an inside corner at the spreading centre. The west flank of the basement high probably forms part of the fault plane, so that the F6 fault extends as far as SP 4940. The heave on the F6 structure is thus ∼ 8 km: this fault accommodated considerable extension and may have exposed deep crustal or even mantle rocks, depending on its initial dip and depth of penetration. Similarly, we trace F7 along top basement as far as SP 4740. Within the basement, F7 can be tentatively traced (partly by discrete fault plane reflections, partly by truncation of other reflection packages) to a depth of 10 km at SP 5150. Strong reflections at ∼ 8 km at the extreme right of the profile appear on the time migration to project up to an offset of top basement, and could be interpreted as coming from a fault plane. However, these reflections have anomalously low velocities from depth-focusing error analysis, are overmigrated on the depth migration and do not project up to a basement offset, and almost certainly a side-coming event.

basement lows, whereas other basement highs (SPs 5230, 5140, 4580, and 4450) are smaller and comparable with the largest observed on Profile B.

Reflections in the basement associated with basement topography generally cut down from the west-facing flank of the highs and dip towards the west (Figs 11 and 12), consistent with an interpretation of the west-dipping slopes as ridgeward-facing flanks of fault blocks bound by west-dipping faults. The quality of the images of the west-dipping features in the crust is variable: some are clearly visible as relatively strong continuous reflections; others are marked by the alignment of shorter reflection segments. For instance a west-dipping feature (F6) can be traced as a series of reflection segments up to the east from a depth of ∼9 km at SP 5300 towards the top of the basement high at SP 4950 (Fig. 11). The reflection approaches the top basement at SP 5100 and is aligned with the west-dipping, slightly convex-up top of the basement between there and SP 4950. The same feature can be identified on the time migration, where it exhibits strong pull-up effects beneath the basement highs at SPs 5200 and 5130 (i.e. it comes from within the basement beneath these basement highs). The geometry of this feature on the time migration is so distorted that without the depth migration it would be hard to interpret west of ∼SP 5190, but on the depth section it can be traced at least 5 km further west (SP 5300) as an approximately linear structure. We interpret this feature (F6) as a fault, and suggest that the co-linear west-facing flank of the basement high represents the continuation of the slip surface as exposed at the seafloor at the spreading centre. F6 apparently dips at about 15° in the crust, but flattens to 10° as it runs into the west-facing flank of the basement high at SP 5100. The feature has a length of at least 10 km in the basement; the associated west-facing basement flank has a length of over 8 km. A local basement high in the hangingwall of F6 at SP 5130 also appears to be flanked by a west-dipping structure

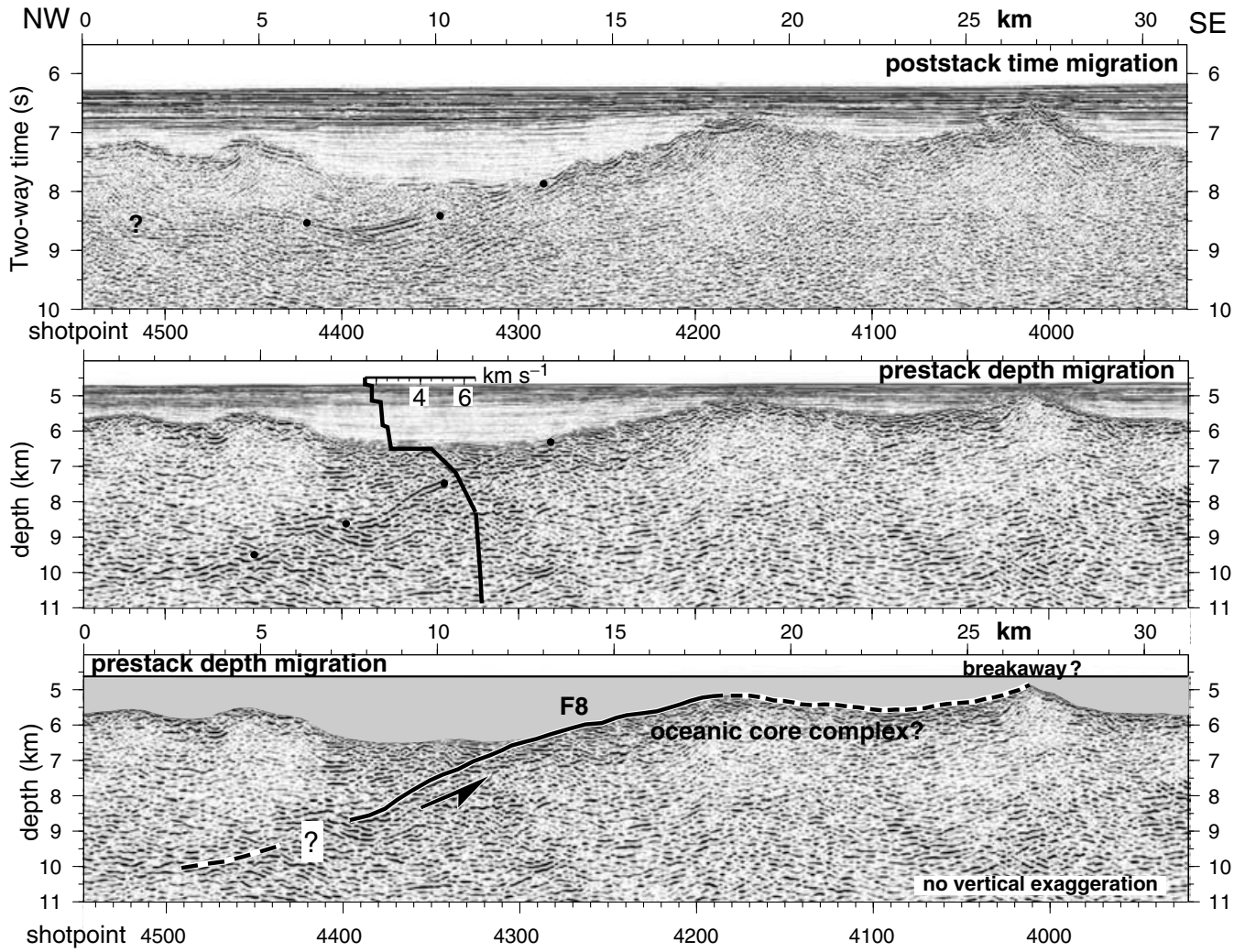

Figure 12. Portion of Profile C. Top: post-stack time migration. Middle: pre-stack depth migration, showing the velocity model used in basement. In general all velocity models from top basement down were similar to this and consistent with the known velocity structure of oceanic crust. Bottom: interpretation. A structure (F8—dots) appears listric on the time migration (A) due to velocity pull-up effects (indicating that the reflection comes from within basement beneath the profile), but on the depth image can be traced as a series of reflection segments from the west flank of a basement high to a depth of at least 9 km. This structure is approximately linear at depth but flattens upwards near top basement. The slip surface to the east follows top basement at least as far east as the basement high at SP 4190, and probably as far as the sharper basement high at SP 4020. We thus infer that the fault heave is at least 6.5 km, and perhaps as much as 15 km. See text for discussion.

(F5) extending down to ∼8 km depth where it merges with the F6 structure. As discussed below, we interpret these structures to be part of a single fault system.

Within the upper few hundred metres of the section beneath our pick of F6 is a patch of reflectivity. This might come from slightly out of the plane of the section (e.g. off a corrugation), or may represent a small perched basin that developed in the west-dipping flank of the basement high. If so this might be an example of a successor basin (e.g. Tucholke & Lin 1994) that developed where the flexure of the exhumed footwall to a large offset fault is accommodated by minor faulting—note that no possible fault can be traced deeper than 0.5 km beneath this patch. If this is indeed a successor basin, it would not affect our interpretation that F6 originally extended to the top of the basement high at SP 4930 (see below), but rather confirm the suggestion that we are here imaging a large-offset normal fault,

Similarly, a west-dipping slightly curved reflection (F7) can be traced from at least 7 km depth (1.5 km beneath top basement) towards the basement high at SP 4750, and probably represents the upper portion of a west-dipping normal fault. The depth to which this feature can be traced within the basement is ambiguous beyond about 7 km (SP 4910): it may continue as a series of discontinuously imaged, west-dipping reflection segments (e.g. 7.5 km depth at SP 4960; 9 km depth at SP 5070) to a depth of up to 10 km (SP 5150, ∼4 km beneath top basement). The continuation of the fault to such depths is supported by the apparent termination against the fault of a group of east-dipping reflections in its footwall at ∼ SP 5000. Overall, the F7 structure appears to approximately parallel F6, dipping west at an angle of ∼ 15°.

F7 is so distorted on the time migration that it is difficult to identify. However, using the depth migration as a guide, F7 can be followed as marked by the dots in Fig. 11(a). It appears to cut down slightly to the west from the offset of top basement, and then up to smaller traveltimes to the west of SP 4860, as a result of the strong velocity pull-up beneath the basement high at SP 4950. Beneath the basement high, it forms a domal feature before increasing in TWT further west still. The east-dipping reflections that are

truncated by F5 in the depth section can also be identified in the time migration as subhorizontal reflections, further illustrating the strong distortions apparent on the time migrations. The strong pull-up effects on the time migrations, and their removal after PSDM with a velocity model tracking top basement do, however, indicate that the reflections imaged are from within the basement below the profile.

F7 is aligned with the convex-up west-facing top of the basement between the basement hangingwall cut-off and SP 4750. The structure is smaller than F6, being traceable for perhaps 4 km in the basement. The length of the associated west-facing flank of the basement high is debatable (see below) but is at least 2 km and may be as much as 5 km.

The west-dipping reflection F8, projecting up towards the west flank of the basement high at SP 4180 (Fig. 12), is better imaged. This reflection exhibits clear pull-up on the time section (Ranero & Reston 1999, see Fig. 12); in depth it initially steepens downwards slightly from top basement, continuing the convex-up shape of the west-facing flank of the basement high. Deeper still, a reflection segment appears to align with the upper structure and may represent part of the same fault system. Over its entire intrabasement extent, the structure has an average dip of $\sim 20^\circ$, and a lateral extent of over 10 km. The structure also follows top basement for at least 5 km (as far east as SP 4180), and as discussed below perhaps for $\sim$ 15 km (as far east as SP 4010).

We interpret the west-dipping structures on Profile C as major normal faults formed at the spreading centre: there is no evidence for faulting within the overlying sedimentary cover, nor evidence of significant syn-faulting deposition as there are no wedges of sediment fanning towards the faults. In all cases, it appears that the west-facing flank of the fault-block actually represents the continuation of the slip surface. The structures resemble oceanic core complexes (Tucholke *et al.* 1998) observed at the flanks of the MAR (Ranero & Reston 1999).

5 DISCUSSION

The profiles we have studied are close to flow-line profiles and cross crust formed between M0 and M16, that is over about 20 Myr in the Early Cretaceous. As faults develop and are active within 10–20 km of the spreading axis, and are subparallel to the ridge axis (Toomey *et al.* 1988; Escartin *et al.* 1999), our depth images (bearing in mind the uncertainties in the interpretation) may provide a partial record of the amount and geometry of extensional faulting close to the spreading centre during this period at various positions within different spreading segments. In this section we discuss briefly the implications of our interpretations for the geometry and style of faulting, the amount of extension, and the depth of exhumation along these faults. Several factors may be important in assessing these characteristics: the extent of the fault surface exposed as top basement, the effect of mass-wasting on this and on the apparent heave and throw of the fault, the initial dip of the faults, and the depth to which the faults reach.

5.1 Estimation of fault geometry

The largest errors in our determination of fault geometry come from the velocity model used, the obliquity of the structures to the profile, and the interpretation made, which is unquantifiable. The main effect of using an incorrect velocity is in the conversion from time to depth, and hence in the dip of key reflectors. We estimate that the error in the determination of fault dip due to velocity inaccuracies is less than 10 per cent. A further correction should be made for the obliquity of the profiles, but as this is less than 15°, the effect is negligible: a fault dipping at 30° will on a 15° oblique profile appear to dip at 29°, which is less than the measurement error for our depth sections. Finally, we do not know the orientation of the faults to the spreading axis. A recent paper (Hallenborg *et al.* 2003) argued that many deep crustal reflections in fast spread crust may actually dip in the isochron direction. However in this paper we are dealing largely with structures related to basement topography, which has been shown by numerous bathymetric studies to be parallel to the spreading axis and thus probably controlled by faults dipping in the flow-line direction. Studies at or near the spreading axis have shown that, although some faults can be oriented as much as 15° to the spreading axis in the middle of the segment (e.g. Shaw & Lin 1993; Escartin *et al.* 1999,—leading to an error in the determination of fault dip of perhaps 3 per cent), most are subparallel to the ridge axis. The general lack of seismic activity away from the ridges makes it unlikely that this topography developed later. Furthermore, the only fault for which we do have proper 3-D control is F4, which dips unequivocally in the direction of the ridge. Unless models for faulting at mid-ocean ridges are totally wrong and the orientation of F4 is atypical, we estimate that the overall error in our determinations of the geometry of most of the faults is probably <10 per cent. Only the faults in the vicinity of the Hierro FZ are likely to be more than slightly oblique to the profiles and so liable to a larger geometrical error. As a result, F1, F2 and F3 may be steeper than their images and may be associated with smaller heaves.

Where possible we have attempted to estimate the original dip of the faults (at the surface) from the angle of intersection of the fault with the top of the footwall and/or the hangingwall. Although these estimates are only approximate, it appears that, on the portion of Profile B studied, most faults initiated at angles of about $45^\circ \pm 10^\circ$. This range is consistent with previous estimates of fault dips at spreading centres from earthquake data (e.g. Toomey *et al.* 1988). On Profile C, the initial dip may have been somewhat lower ($35^\circ \pm 10^\circ$).

5.2 Extent of the exposed slip surface and amount of fault-controlled extension

The minimum extent of the fault in the basement can be partly recognized from the seismic data (fault plane reflections, truncation of other structures), but in places the faults may be seismically invisible. As a result, the dimensions of the faults within basement discussed above and listed in Table 1 may be an underestimate.

The upper part of the slip surface of all normal faults is exposed as the exhumed footwall and is one way to distinguish between genuine faults offsetting top basement by several hundreds of metres and fractures (e.g. Hallenborg *et al.* 2003), which, although perhaps of similar dimensions within basement, should not significantly offset basement. This aspect of fault geometry is of particular interest as the heave at top basement level is related to the amount of displacement along the fault. The criteria for recognising this slip surface on the seismic sections are the co-linearity of the top of basement with the dipping fault imaged within the basement, and in some case the continuation of the curvature of the fault as top basement. As most of the faults imaged are west-dipping features, the west-facing flanks of the basement ridges are the main candidates for exhumed slip surfaces. Their extent depends on the recognition of the original intersection of the fault with the top of the footwall, the breakaway.

Table 1. Characteristics of main faults based on depth imaging of portions of Profiles B and C. Asterisks: F3, F5—measurements of extent of fault are to point of merger with F2, F6 respectively; D detachments: original dip at top basement determined from footwall breakaway, possibly less at depth if D1, D2 originated as listric structures; maximum amounts of extension that could be inferred by restoring the lower plate to an initial dip of 45°—we believe this to be an overestimate. Exhumations for F6 and F8 assume that faults cut deeper than imaged; otherwise maximum exhumation will be reduced. HW = hangingwall; TB = top basement.

Fault	F1	F2	F3	F4	D1	D2	F5	F6	F7	F8
Profile	B	B	B	B	B	B	C	C	C	C
SP (at HW cut-off)	2530	2670	2760	3820	1760	2200	5160	5070	4860	4320
Mean dip in crust (°)	40	40	15	45	−5 to 20	5 to 20	25	15	15	20
Estimate of original dip	54	45	>30	47	35	<45	45	25–30	20–40	35–40
Length in crust (km)	7	5	5.5 *	6.5	10	10–12.5	3	>12	15	10
Max. depth beneath TB (km)	5.5	3.5	1.5 *	5	2.5	3–5	2*	3	3.5	4
Heave (min–max) (km)	0.5	0.6	2.2–2.8	1.5–2.0	1–6*	0.7–6*	1.5	8	2.2–5	6.5–15
Throw (km)	0.5	0.5	0.5	1.5–1.0	0.8	0.5	0.6	1.2	1	1.5–2
Exhumation (km): 45°	0.5	0.5	2	1.5–1.0	0.8	0.5		6	1.8–3.7	4.5–10
and 30° initial dip assumed	—	—	1.25	—				4.3	1.3–2.6	3–7

This is in some cases fairly unambiguous: for instance, the west-facing scarp co-linear with the intrabasement portion of fault F2 is a continuous surface that ends abruptly at the top of the fault block (e.g. Fig. 5, SP 2700). In other cases, the identification of the breakaway is unclear, in part because of the effects of mass-wasting and flexure.

Mass-wasting (e.g. Tucholke *et al.* 1997b) may particularly affect the steeper faults characteristic of Profile B. For instance, at SP 2540 the corner of the basement between the top of the footwall and fault F1 (Fig. 5) appears to be missing. The footwall to F4 (Fig. 7) may also have undergone mass-wasting as discussed above, with two consequences for the estimate of heave (Escartin *et al.* 1999 Fig. 7). First, mass-wasting may cause the scarp to retreat into the hangingwall, increasing the measured heave. Conversely, the products of mass-wasting may collect as a rubble zone burying the base of the fault scarp (e.g. wedge-shaped unit in Fig. 7). On side-scan sonar data, the misinterpretation of a talus slope as a fault surface may lead to a further overestimation of the heave (Escartin *et al.* 1999). On the seismic data, the geometry of the fault at depth is imaged, so it is unlikely that a talus slope extending away from the exposed fault would be identified as the fault surface; instead slide deposits may lead to an overestimate of the height of the hangingwall basement, reducing the apparent heave of the fault (Fig. 7). Because of these possible inaccuracies we have used a range of possible vertical throws of the fault and an estimate of the fault dip from that observed within the basement to calculate heave (Table 1) for those faults where mass-wasting appears to have been a problem.

The other west-facing flanks of the highs on Profile B appear to continue the dip and curvature of the faults in the basement, without any abrupt discordance between the angle of the fault at depth and the slope of the west-facing flank. Furthermore, no mass-wasting deposits are imaged. For these faults (e.g. F3), we propose that any flattening of the fault dip above top basement is a consequence of the flexure of the footwall in response to the removal of the hangingwall load. As the slip surface forms much of the west-facing slope to the basement highs, we use the dimensions of the west-facing slope to estimate fault displacement.

The faults imaged along Profile C extend for up to 10 km in the basement and are associated with basement offsets up to 2 km high (Table 1). The faults dip at less than 25° within the basement and appear to flatten upwards near top basement. This flattening appears to continue as the convex-up geometry of the associated ridgeward-dipping flanks of the basement highs (e.g. Figs 11 and 12), which we thus interpret as slip surfaces on the exhumed footwall. It is improbable that the large faults imaged on Profile C continued as steeper structures and that the current west-facing slope is the result of erosion and mass-wasting of an originally steeper fault scarp. First, the ridgeward-facing slopes of the basement highs are typically convex-up (e.g. Fig. 11, SP 4950; Fig. 12, SP 4200), whereas mass-wasting generally produces concave-up slopes (e.g. Tucholke 1992). Second, the faults on Profile C are relatively low-angle, and the basement highs on Profile C are also characterized by relatively low-angle flanks, which would not be very susceptible to mass-wasting—they are less steep than the mass-wasted scarps described by Tucholke *et al.* (1997b). Finally, the observation of corrugated megamullion structures a considerable distance off-axis and partly buried by sediment (e.g. Tucholke *et al.* 1997a; Reston *et al.* 2002) implies that such structures can survive off-axis without significant modification by mass-wasting.

The identification of the breakaway on Profile C is, however, problematic as the faults only intersect the top of the footwall at low angle. Furthermore, the convex-up flattening of the fault block (due to flexural unloading) means that the top of the basement high is characterized by a subhorizontal region rather than a clear peak (e.g. Fig. 11, SPs 4720–4780). As the breakaway is the original intersection of the west-dipping fault with top basement before rotation, it should correspond to the sharpest change in slope of top basement consistent with a moderate initial fault dip towards the spreading axis. On this basis, we suggest that F7 extends to SP 4750, where the broad basement high ends in an *east-dipping* scarp. This geometry can be explained by the flexural rotation of a large-offset normal fault (Buck 1988; Lavier *et al.* 1999) that dipped towards the median valley.

Particularly intriguing is the eastward extent of the F8 fault plane on Profile C (Fig. 12). The fault plane can be taken along the smooth convex-up shape of the west-facing flank of the basement high at least as far as the peak of that high at SP 4180. However this high is somewhat domal, and the fault plane may continue over the dome and down the other side of the high, eventually reaching a breakaway at the top of the sharper basement high immediately to the east, that is at SP 4020. We note that there is no west-dipping reflection cutting down from top basement at the centre of the basin between the two highs (∼SP 4100), supporting the idea that the eastern basement high (SP 4020) may actually be part of the F8 fault system, and the high at SP 4180 an oceanic core complex to the F8 structure, similar to the oceanic core complexes described near the spreading axis (Cann *et al.* 1997; Tucholke *et al.* 1998). Where a breakaway has been identified for oceanic core complexes (Tucholke *et al.* 1998),

the overall geometry closely resembles that in Fig. 12 (Ranero & Reston 1999). Placing the breakaway to F8 as far east as SP 4020 increases the heave, the amount of extension and the implied depth of exhumation considerably (Table 1 and see below). However, the magnitudes are fully consistent with observations of ICs made near the spreading axis (Ranero & Reston 1999) and with the predictions of numerical modelling (Lavier *et al.* 1999).

Our analysis assumes that the faults strike normal to the profile and as such are likely to overestimate the heaves slightly: if the faults strike parallel to the ridge, the overestimate should be ∼4 per cent; if the faults are up to 15° off ridge-parallel, then the estimate may be up to 14 per cent too high. Even allowing for these possible errors, the heaves estimated in this way suggest that there is considerably more extension along Profile C than along Profile B (Table 1), supporting the interpretation that Profile C runs along tectonically extended inside corner crust and Profile B follows less faulted, more magmatic crust. Similarly, the depth of exhumation (Table 1) that can be deduced from the large-scale faults along Profile C is considerably greater than for any of the faults on Profile B and provides a mechanism for the unroofing and exposure of deep crustal and perhaps even mantle rocks along Profile C. This is consistent with the geology of inside corner highs.

5.3 Comparison with previous results

Previous studies of faulting in Mesozoic Atlantic oceanic crust have been based on three data sets: a large loose grid in the Blake Spur region (Morris *et al.* 1993), and tighter but smaller grids in the Cape Verde Abyssal Plain (White *et al.* 1994; McBride *et al.* 1994; Reston *et al.* 1996b) and in one part of the Canary Basin (Collier *et al.* 1998). The data set presented here is complementary to the latter two data sets (also from the eastern Central Atlantic), providing more information on the variation in structure with time, and imaging similar structures. The D detachments resemble structures observed on the BIRPS OCEAN data in the Cape Verde Abyssal Plain— Reston *et al.* (1996b). In some cases, we have studied the same structure as previous studies [for example F4 and the landward-dipping lower crustal reflections on Profile B between SPs 3400 and 3900 were also investigated by Collier *et al.* (1998), but with a rather different emphasis]. However, neither the BIRPS nor the Collier data sets provides images of large, low-angle convex-up structures (F6–F8) similar to those imaged on Profile C.

The pattern of faulting evident on all three data sets from the eastern Central Atlantic differs markedly from the data in the Blake Spur region. There crustal-scale faults (e.g. Mutter & Karson 1992; Morris *et al.* 1993) appear concave-up on flow-line profiles, steepen upwards to dip >45° in the upper crust, and are associated with little basement topography. The Blake Spur structures also do not explain observations made at modern inside corners (Tucholke & Lin 1994). Minshull (1999) demonstrates that the Blake Spur crust is smoother and slightly thicker than most crust formed recently at the MAR at similar spreading rates. He concludes that the Blake Spur region is not typical of crust formed at slow-spreading rates and was possibly influenced by a mantle thermal anomaly during accretion so that the tectonism was similar to hotspot-influenced slow-spreading ridges. In contrast, basement roughness on most of our data and on the flanks of the MAR is comparable (Minshull 1999). Only the region of smooth basement between F3 and F4 on Profile B resembles the Blake Spur data: both are characterized by slightly thick crust (∼8 km— Collier *et al.* 1998; Minshull 1999) and by enigmatic LCDRs.

6 CONCLUSIONS

We have presented depth images from two seismic profiles, one over slow-spread Cretaceous crust formed at the inside corner of a 30-km offset transform fault, the other over crust of the same age formed at similar spreading rates away from transform faults but crossing the projected trace of a SOFZ at a low angle. The depth images reveal for the first time the true geometry of major faults and the relationship between the faults and top basement.

Based on these data we recognisze three main types of faults that probably developed at the spreading centre. The different fault types reflect different amounts of extension, consistent with different positions within the spreading segment.

(1) Relatively steep, deeply penetrating faults form away from major fracture zones. We suggest that these faults are imaged in crust where more magmatic extension dominated and faulting accommodated little extension, but rather served to lift newly formed crust out of the median valley (Shaw & Lin 1993). It appears that these faults mostly formed at an angle of 45° ± 10°

(2) Possible low-angle detachment faults are also imaged away from major fracture zones. Similar features are observed on the BIRPS OCEAN data (Reston *et al.* 1996b). The middle portions of these structures are currently subhorizontal, but may have been active only at steeper angles and have subsequently been passively rotated to low angles as a rolling hinge. Further along from the breakaway, the structures steepen into a root zone that dips at 20°–30°, which may represent the angle at which the structures were active if they developed as a rolling hinge.

(3) Large-scale, low-angle faults currently dipping at ∼20° develop in crust formed at an IC (marked by an elongated gravity high to a 30-km offset transform fault. These faults root deep in the crust, may have formed at ∼35°–40°, and appear to continue as top basement for considerable distances, in places possibly passing over domal highs to breakaways further away from the spreading centre. Movement along these faults may have accommodated up to 50 per cent of the extension occurring at the spreading centre, and may have resulted in the exhumation of deep crustal and mantle rocks. These structures may correspond to the corrugated slip surfaces identified on active inside corner highs (Cann *et al.* 1997): the domal corrugated slip surfaces are in effect oceanic core complexes (Tucholke *et al.* 1998) where peridotites and gabbros have been sampled. These structures continue at low angle for 10–15 km in the basement, sufficient to have reached beneath the centre of the median valley where any magma may have accumulated at ∼5 km below top basement.

ACKNOWLEDGMENTS

This work was supported by the Deutsche Forschungsgemeinschaft (DFG) under grant Re 873/4, which we gratefully acknowledge. JJD was funded by the EC Human Capital and Mobility program (CHGE-CT93–0025). Dirk Klaeschen provided technical help during the course of this work. Ingo Grevemeyer commented on an earlier version of the manuscript; Yves Lagabrielle and the third reviewer provided constructive and detailed comments.

REFERENCES

Agar, S. & Klitgord, K., 1995. A mechanism for decoupling within the oceanic lithosphere revealed in the Troodos ophiolite, *Nature,* **374**, 232–238.

Allerton, S. & Vine, F., 1987. Spreading structure of the Troodos ophiolite, Cyprus: Some paleomagnetic constraints, *Geology,* **15**, 593–597.

Banda, E., Ranero, C.R., Dañobeitia, J.J. & Rivero , A., 1992. Seismic boundaries of the eastern central Atlantic Mesozoic crust from multichannel seismic data, *Geol. Soc. Am. Bull.,* **104**, 1340–1349.

Bergman, E.A. & Solomon, S.C., 1984. Source mechanisms of earthquakes near mid-ocean ridges from body waveform inversion: Implications for the early evolution of oceanic lithosphere, *J. geophys, Res.,* **89**, 11 415–11 441.

Buck, W.R., 1988. Flexural rotation of normal faults, *Tectonics,* **7**, 959–973.

Cann, J.R. *et al.,* 1997. Corrugated slip surfaces formed at ridge-transform intersections on the Mid-Atlantic Ridge, *Nature,* **385**, 329–333.

Cannat, M., 1996. How thick is the magmatic crust at slow-spreading ridges?, *J. geophys. Res.,* **101**, 2847–2857.

Cannat, M. *et al.,* 1995. Thin crust, ultramafic exposures and rugged faulting patterns at the Mid-Atlantic Ridge (22°–27°), *Geology,* **23**, 49–52.

Carbotte, S.M. & Macdonald, K.C., 1990. Causes of variation in fault-facing direction on the ocean floor, *Geology,* **18**, 749–752.

Collier, J.S. *et al.,* 1997. Evidence for asymmetric accretion and low-angle, planar faults in slow-spreading oceanic crust, *Geology,* **25**, 1075–1078.

Collier, J.S., Henstock, T.J., Peirce, C. & Watts, A., 1998. A detailed geophysical study in the Canary Basin (eastern Atlantic); implications for the internal structure of 130 Ma oceanic crust, *Geophys. J. Int.,* **135**, 943–963.

Denelle, E., Dezard, Y. & Raoult, J., 1986. 2-D pre-stack depth migration in the (S-G-W) domain. Extended abstract, in 56th SEG Meeting, Houston, pp. 327–330, Society of Exploration Geophysicists, Tulsa, OK, USA.

Detrick, R.S., Mutter, J.C., Buhl, P. & Kim, I.I., 1990. No evidence from multichannel reflection data for a crustal magma chamber in the MARK area of the Mid-Atlantic Ridge, *Nature,* **347**, 61–64.

Dilek, Y., Moores, E.M. & Furnes, H., 1998. Structure of modern oceanic crust and ophiolites and implications for faulting and magmatism at oceanic spreading centers, *Am. geophys. Un. Monogr.,* **106**, 219–265.

Escartin, J., Cowie, P.A., Searle, R.C., Allerton, S., Mitchell, N.C., MacLeod, C.J. & Slootweg, A.P., 1999. Quantifying tectonic strain and magmatic accretion at a slow spreading ridge segment, Mid-Atlantic Ridge, 29 degrees N, *J. geophys. Res.,* **104**, 10 421–10 437.

Gente, P. *et al.,* 1995. Characteristics and evolution of the segmentation of the Mid-Atlantic Ridge between 20 degrees N and 24 degrees N during the last 10 million years, *Earth planet Sci. Lett.,* **129**, 55–71.

Hallenborg, E., Harding, A.J., Kent, G.M. & Wilson, D.S., 2003. Seismic structure of 15 Ma oceanic crust formed at an ultrafast spreading East Pacific Rise: Evidence for kilometer-scale fracturing from dipping reflectors, *J. geophys. Res.,* **108**, 2532, doi:10.1029/2003JB002400

Henstock, T.J., White, R.S. & McBride, J.H., 1996. Along-axis variability in crustal accretion at the Mid-Atlantic Ridge; results from the OCEAN study, *J. geophys. Res.,* **101**, 13 673–13 688.

Huang, P.Y. & Solomon, S.C., 1988. Centroid depths of mid-ocean ridge earthquakes: Dependence on spreading rate, *J. geophys. Res.,* **93**, 13 445–13 477.

Kent, D.V. & Gradstein, F.M., 1985. A Cretaceous and Jurassic geochronology, *Geol. Soc. Am. Bull.,* **96**, 1419–1427.

Kent, G.M., Kim, I.I., Harding, A.J., Detrick, R.S. & Orcutt, J.A., 1996. Suppression of sea-floor-scattered energy using a dip-moveout approach; application to the mid-ocean ridge environment, *Geophysics,* **61**, 821–834.

Lagabrielle, Y. & Cannat, M., 1990. Alpine Jurassic ophiolites resemble the modern central Atlantic basement, *Geology,* **18**, 319–322.

Lagabrielle, Y., Bideau, D., Cannat, M., Karson, J.A. & Mevel, C., 1998. Ultramafic-mafic plutonic rock suites exposed along the Mid-Atlantic Ridge (10 degrees N-30 degrees N); symmetrical-asymmetrical distribution and implications for seafloor spreading processes, *Am. geophys. Un. Monogr.,* **106**, 153–176.

Lavier, L.L., Buck, W.R. & Poliakov, A.N.B., 1999. Self-consistent rolling-hinge model for the evolution of large-offset low-angle normal faults, *Geology,* **27**, 1127–1130.

Lister, G.S. & Davis, G.A., 1989. The origin of metamorphic core complexes and detachment faults during Tertiary continental extension in the northern Colorado River region, U.S.A., *J. struct. Geol.,* **11**, 65–94.

McBride, J.H., White, R.S., Henstock, T.J. & Hobbs, R., 1994. Complex structure along a Mesozoic sea-floor spreading ridge: BIRPS deep seismic reflection, Cape Verde Abyssal Plain, *Geophys. J. Int.,* **119**, 453–478.

McCarthy, J., Mutter, J.C., Morton, J.L., Sleep, N.H. & Thompson, G.A., 1988. Relic magma chamber structures preserved within the Mesozoic North Atlantic crust?, *Geol. Soc. Am. Bull.,* **100**, 1423–1436.

Macdonald, K.C., Scheirer, D.S. & Carbotte, S.M., 1991. Mid-ocean ridges: discontinuities, segments and giant cracks, *Science,* **253**, 986–994.

Minshull, T.A., 1993. Wide-angle imaging of reflectors in Mesozoic oceanic crust, *Geophys. Res. Lett.,* **20**, 1619–1622.

Minshull, T.A., 1999. On the roughness of Mesozoic oceanic crust on the Western North Atlantic, *Geophys. J. Int.,* **136**, 286–290.

Mitchell, N., Escartin, J. & Allerton, S., 1998. Detachment faults at mid-ocean ridges garner interest, *EOS, Trans. Am. geophys. Un.,* **79**, 127.

Morris, E., Detrick, R.S., Minshull, T.A., Mutter, J.C., White, R.S., Su, W. & Buhl, P., 1993. Seismic structure of oceanic crust in the western North Atlantic, *J. geophys. Res.,* **98**, 13 879–13 903.

Mutter, J.C. & Karson, J.A., 1992. Structural processes at slow spreading ridges, *Science,* **257**, 627–634.

Ranero, C.R. & Reston, T.J., 1999. Detachment faulting at ocean core complexes, *Geology,* **27**, 983–986.

Ranero, C.R., Banda, E. & Buhl, P., 1997. The crustal structure of the Canary Basin: Accretion processes at slow spreading centres, *J. geophys. Res.,* **102**, 10 185–10 201.

Reston, T.J., Krawczyk, C.M. & Klaeschen, D., 1996a. The S reflector west of Galicia: Evidence from pre-stack depth migration for detachment faulting during continental breakup, *J. geophys. Res.,* **101**, 8075–8091.

Reston, T.J., Ruoff, O., McBride, J.H., Ranero, C.R. & White, R.S., 1996b. Detachment and steep faulting in the oceanic crust west of Africa, *Geology,* **24**, 811–814.

Reston, T.J., Ranero, C.R. & Belykh, I., 1999. The structure of Cretaceous oceanic crust of the NW Pacific: Constraints on processes at fast spreading centres, *J. geophys. Res.,* **104**, 629–644.

Reston, T.J. *et al.,* 2002. A Rifted Inside Corner Massif on the Mid-Atlantic Ridge at 5°S, *Earth planet. Sci. Lett.,* **200**, 255–269.

Roest, W.R., Dañobeitia, J., Verhoef, J. & Collette, B.J., 1992. Magnetic anomalies in the Canary Basin and the Mesozoic evolution of the Central North Atlantic, *Mar. Geophys. Res.,* **14**, 1–24.

Schouten, H. & White, R.S., 1980. Zero-offset fracture zones, *Geology,* **8**, 175–179.

Shaw, P.R. & Lin, J., 1993. Causes and consequences of variations in faulting style at the Mid-Atlantic Ridge, *J. geophys. Res.,* **98**, 21 839–21 851.

Smith, D.K. & Cann, J.R., 1990. Hundreds of small volcanoes on the median valley floor of the Mid-Atlantic Ridge at 24–30_N, *Nature,* **348**, 152–155.

Smith, W.H.F. & Sandwell, D.T., 1995. Marine gravity field from declassified Geosat and ERS-1 altimetry (abstract), *EOS, Trans. Am. geophys. Un.,* **76**(46), Fall Mtg Suppl., F156.

Solomon, S.C., Huang, P.Y. & Meinke, L., 1988. The seismic moment budget of slowly-spreading ridges, *Nature,* **334**, 58–60.

Spudich, P. & Orcutt, J., 1980. A new look at the seismic velocity structure of the oceanic crust, *Rev. Geophys. Space Phys.,* **18**, 627–645.

Toomey, D.R., Solomon, S.C. & Purdy, G.M., 1988. Microearthquakes beneath the median valley of the Mid-Atlantic Ridge near 23°N: Tomography and tectonics, *J. geophys. Res.,* **93**, 9093–9112.

Tucholke, B.E., 1992. Massive submarine rockslide in the rift-valley wall of the Mid-Atlantic Ridge, *Geology,* **20**, 129–132.

Tucholke, B. & Lin, J., 1994. A geological model for the structure of ridge segments in slow spreading oceanic crust, *J. geophys. Res.,* **99**, 11 937–11 958.

Tucholke, B.E., Lin, J., Kleinrock, M.C., Tivey, M.A., Reed, T.B., Goff, J. & Jaroslow, G.E., 1997a. Segmentation and crustal structure of the western Mid-Atlantic Ridge flank, 25°25′ –27°10′ N and 0–29 m.y., *J. geophys. Res.,* **102**, 10 203–10 223.

Tucholke, B.E., Stewart, W.K. & Kleinrock, M.C., 1997b. Long-term denudation of ocean crust in the central North Atlantic Ocean, *Geology,* **25**, 171–174.

Tucholke, B.E., Lin, J. & Kleinrock, M.C., 1998. Megamullions and mullion structure defining oceanic metamorphic core complexes on the Mid-Atlantic Ridge, *J. geophys. Res.,* **103**, 9857–9866.

Verhoef, J., Roest, W., Macnab, R., Arkani-Hamed, J. & members of the project team, 1996. *Geol. Survey Canada, open file,* 3125b. Geol. Survey Canada, Calgary, Alberta, Canada.

White, R.S., Detrick, R.S., Mutter, J.C., Buhl, P., Minshull, T.A. & Morris, E., 1990. New seismic images of oceanic crustal structure, *Geology,* **18**, 462–465.

White, R.S., McKenzie, D.P. & O'Nions, R.K., 1992. Oceanic crustal thickness from seismic measurements and rare earth element inversions, *J. geophys. Res.,* **97**, 19 683–19 715.

White, R.S., McBride, J.H., Henstock, T.J. & Hobbs, R.W., 1994. Internal structure of Mesozoic oceanic crust, *Geology,* **22**, 597–600.